Sidechain control of porosity closure in multiple peptide-based porous materials by cooperative folding

C. Martí-Gastaldo[1], D. Antypov[1], J. E. Warren[1], M. E. Briggs[1], P. A. Chater[1], P. V. Wiper[1], G. Miller[1], Y. Z. Khimyak[1,2], G. R. Darling[1], N. G. Berry[1], M. J. Rosseinsky[1]*

[1]Department of Chemistry, University of Liverpool, Liverpool, L69 7ZD, UK; [2] School of Pharmacy, University of East Anglia, Norwich, NR4 7TJ

Abstract

Porous materials find application in separation, storage and catalysis. We report a crystalline porous solid formed by coordination of metal centres with a glycylserine dipeptide. We prove experimentally that the structure evolves from a solvated porous into a non-porous state as result of ordered displacive and conformational changes of the peptide that suppress the void space in response to environmental pressure. This cooperative closure, which recalls the folding of proteins, retains order in three-dimensions and is driven by the hydroxyl groups acting as H-bond donors in the peptide sequence through the serine residue. This ordered closure is also displayed by multipeptide solid solutions in which the combination of different sequences of amino acids controls their guest response in a non-linear way. This functional control can be compared to the effect of single point mutations in proteins, where the exchange of single amino acids can radically alter structure and function.

Introduction

Metal-Organic Frameworks (MOFs) are a class of crystalline, microporous materials built up from the combination of metal ions or clusters with organic linkers.[1] Their intrinsic porosity and the presence of metal sites confer interesting properties on these solids of use in gas storage and separation,[2,3] heterogeneous catalysis,[4,5] drug delivery[6] or sensing,[7,8] amongst a range of applications. Furthermore, their rich structural diversity, generally controlled by the topology and denticity of the organic synthon, enables access to pores of variable size[9,10] or fine-tuning of their physical behaviour by the introduction of functional organic sites (FOS) that decorate the pore walls and tune the guest-to-framework interaction.[11] These systems thus offer chemically controllable ordered porosity because of the functional role of the organic linker in determining the internal surface chemistry and the structural response to guests.

Biologically derived linkers such as amino acids (aa's)[12] or nucleobases[13] have proven successful in the synthesis of MOFs.[14] These molecules afford extensive chemical functionality, including chirality and versatile metal binding modes. Peptides are a particularly diverse set of candidate linkers within this class because of the array of sidechain chemistries and the role of amino acid residue sequence in controlling their behaviour.

Peptides differ from classical rigid aromatic-based MOF linkers in the extensive conformational space accessible through low-energy torsions. Such modes enable protein folding, which can take place in an ordered manner between well-defined structures involving large atomic displacements, in response to environmental changes.[15] The torsional manifold of the peptide chains, controlled by the nature and sequence of the amino acid residues,

allows the required conformations to be accessed, thereby enabling key biochemical processes. As the torsional response of an oligopeptide chain, though by definition less complex than that of a protein, is also controlled by the amino acid sequence, there is an opportunity to use these motions, and any translational displacements they may enable, to control the guest response of a MOF. The disordered torsional response of GA in Zn(Gly-Ala)$_2$ closes the pore space upon guest removal.[16] Here, changes in the torsions of the peptide linker adapt the pore morphology in response to the presence of guests. This contrasts with the classical rigid behaviour of Zn(Gly-Thr)$_2$,[17] which is a robust permanently porous material whose structure is invariant to the presence or nature of guests. Unlike Gly-Ala (GA), Gly-Thr (GT) is conformationally invariant, as it forms a chelate to Zn^{2+} and establishes additional H-bonds mediated by the –OH groups in the Thr side-chain which are of course inaccessible to the -CH_3 of Ala. These examples demonstrate the critical role of the sidechain in controlling how the torsional degrees of freedom can be deployed in response to environmental changes. Exploiting the torsional space accessible to the peptide linker within an open framework to induce an ordered and controlled structural response to guests more directly analogous to the changes undergone by proteins remains a challenge. We show that changing one dipeptide residue in the linker to form Gly-Ser (GS) allows ordered torsional change and displacement upon guest loss to effect reversible closure of the pores controlled by the side chain hydrogen bonding in Zn(Gly-Ser)$_2$ and coupled to large ordered displacements of the peptide linkers that reversibly suppresses 90% of the initial pore volume. The Ser sidechain retains the –OH functionality of Thr but the change from a secondary to a primary alcohol is sufficient to produce this dramatic change in guest response. The construction of multiple GlyX dipeptide frameworks from the three X residues whose sidechains each impose distinct functions is then demonstrated to control the overall cooperative MOF response in a tuneable way via peptide torsions and sidechain chemistry, attaining responses that are not linear combinations of the end-member single peptide materials. The incorporation of multiple peptides in an MOF framework to control function has analogy with the role of the much more complex and better-ordered amino acid sequences in controlling protein behaviour.

Results and discussion

Solvothermal reaction of zinc (II) nitrate with glycylserine in a methanolic solution slightly basified with NaOH(aq) 1M yields prismatic colorless crystals of [Zn(Gly-Ser)$_2$]•2CH_3OH ($ZnGS_2$), which crystallize in the chiral monoclinic space group $P2_12_12$ (Flack parameter=0.00(2)). $ZnGS_2$ is isostructural to [Zn(Gly-Ala)$_2$]•(solvent) ($ZnGA_2$),[16] and can be described as a chemically modified analogue that incorporates hydroxyl (–OH) groups in the α-carbon position of the C-terminus residue of the oligopeptide. The primary –OH sidechain thus imposes a different structure than that found for the Thr secondary –OH in Zn(Gly-Thr)$_2$ ($ZnGT_2$).[17] $ZnGS_2$ is a 2D layered MOF built from the stacking of neutral [Zn(Gly-Ser)$_2$] square-like sheets. The sheets are formed by tetrahedral Zn^{2+} ions that are linked to four peptides acting as μ_2-bridges. Following the same metal-to-peptide connectivity displayed by $ZnGA_2$, each peptide binds two metal ions through the terminal amino and the monodentate carboxylate groups from the N-term Gly and C-term Ser residues, respectively, imposing intralayer metal-to-metal separations of 10.1615(5) (edge) and 14.0129(10) & 14.6036(10)Å (diagonal) (Fig.1a,b). The dipeptide GS adopts a conformation with torsion angles of -140.0(3) and 166.0(3)º for glycyl (Φ) and serine (Ψ), respectively (SI22). The orientation of the –OH group from the Ser sidechain is determined by H-bonding to the MeOH guest (O1A···H9A, 1.92601(9)Å; Fig.SI10). This is quite different from $ZnGA_2$ or $ZnGT_2$ where the absence (GA) or ability of -OH groups from Thr to form more favourable inter and intraframework H-bonds with C-term carboxylate and N-term amino groups prevent guest-to-

framework sidechain H-bonds (Fig.SI11). The [Zn(Gly-Ser)$_2$] layers are stacked along the *c* axis in an ..AA.. pattern controlled by interlayer H-bonds between peptides in neighbouring layers in a β–sheet mode (Fig.1c), affording isolated 1D channels occupied by MeOH guests.

Removal of the guest generates 1D channels that are oriented along [001] and give a solvent accessible volume of 27.7% (267.6Å^3 at 100K per unit cell; Fig.1d & SI23). This value is larger than the 13.6% reported for ZnGT$_2$, but almost equivalent to that of isostructural ZnGA$_2$ (30%), despite the bulkier nature of the –CH$_2$OH side chain of L-serine over the –CH$_3$ group in L-alanine. The sidechain has a more pronounced impact though on the morphology of the channels. Connolly surfaces display periodic constrictions as result of the orientation of the –OH groups from opposite dipeptides in the layer, which point towards the centre of the channels and impose a more acute bilobal "hourglass" shape on the void space than in ZnGA$_2$ (Fig.1e).

CHN and thermogravimetric analyses (TGA) reveal the presence of two MeOH molecules per unit formula in the as-made solid (SI12), in good agreement with the composition refined from the SCXR data. Phase purity of solvated ZnGS$_2$ is confirmed by powder X-ray diffraction (PXRD; Fig.5e).

ZnGS$_2$ thus has the same structure as ZnGA$_2$ but with different sidechain functionality, suggesting that multiple peptide linkers could be used in the construction of a single framework through the formation of solid solutions using all three dipeptide linkers. Multiple topologically similar linkers have been used to form solid solutions in classical rigid MOF systems[18,19,20,21]. We accessed the solid solutions Zn(X_xY_{1-x})$_2$ (X,Y=GA,GS,GT; 0≥x≥1) and Zn($GA_{0.33}GS_{0.33}GT_{0.33}$)$_2$ using the synthesis procedure for the single peptides modified to afford peptide solutions as reagents and thus enable high-throughput synthesis (SI1). Lightly basified methanolic solutions containing the peptides and the metal precursor were dispensed with a liquid handling robot to guarantee high reproducibility and better control of the experimental ratio of the linkers in the reaction mixture. Solvothermal reaction yields colorless crystals with yields from 65 to 80%. The experimental ratio of dipeptides in the isolated solids was assessed with ^{1}H-NMR of the solutions obtained from digesting freshly made crystals in D$_2$O. The values summarized in SI14 are in good agreement with the theoretical ratio present in the starting solutions. This suggests that there is no preferential affinity of the metal for any of the dipeptides and that dipeptide connectors are perfectly suited for the synthesis of multiple-linker MOFs. Bulk phase purity was confirmed with PXRD (SI35-48). All compounds are isostructural with ZnGX$_2$ (X=Ala,Ser) or ZnGT$_2$ (Fig.SI49), with the topology of the framework being fixed by the relative peptide-to-peptide ratio. Whereas GA(33):GS(33):GT(33) and all GA:GS ratios result in ZnGS$_2$-like topologies, the introduction of GT drives the formation of solids with the ZnGT$_2$ structure for levels of GT doping ≥ 75% in the GA:GT family and ≥ 50% in the GS:GT series, with the ZnGS$_2$ structure adopted at lower substitution levels. The formation of the ZnGS$_2$ structure between isostructural GA and GS frameworks is unsurprising, but the higher GA than GS concentration required to sustain this topology in the presence of GT demonstrates the role of the GS to guest hydrogen bonding in favouring the formation of this structure. The methyl of the Ala sidechain is less effective in overcoming the structure direction by the Thr sidechain alcohol as it makes weaker and less directional intermolecular interactions. The successful synthesis of solid solutions extends the range of functionality displayed by the pore walls in the two distinct structures. SCXR analyses of as-made crystals of ZnGA(50)GS(50), ZnGA(50)GT(50) and ZnGS(50)GT(50) (SI15-18) reveal that the distinct functionalities are homogeneously distributed across the backbone of the multipeptide MOFs. They show local crystallographic disorder affecting the α-carbon position of the C-terminal amino acid as result of the distinct side-chains born by each GlyX dipeptide, with good agreement between the refined occupancy factors used to model the disorder and the experimental linker ratio

extracted from NMR analysis. This is also the case for ZnGS(75)GT(25), which is isostructural with $ZnGS_2$.

Examination of the guest response of Zn-GS(75)GT(25) demonstrates the effect of the hydrogen bonding from the OH sidechains on the behaviour of the $ZnGS_2$ structure. Removal of guests from isostructural $ZnGA_2$ produces extensive local torsional disorder of the GlyAla dipeptide as shown by solid-state ^{13}C cross-polarization/magic angle spinning nuclear magnetic resonance (CP/MAS NMR).[16] Desolvation of ZnGS(75)GT(25) is also possible, but here NMR demonstrates the extremely ordered nature of the solvated and desolvated states at a local level (Fig.2a). The solvated solid displays equivalent environments for the GS/GT amino acids at 179.3, 171.1 and 44.3 ppm that can be assigned to carboxylate, carbonyl and the $–CH_2-$ group adjacent to the amine. Resonances in a 3:1 ratio at 65.4, 55.1, 68.8 and 57.9 ppm are attributed to the inequivalent $–CH_2-$ and –CH- groups in the GS and GT amino acids respectively, consistent with the GS(75):GT(25) ratio. The presence of MeOH is confirmed by the resonance at 50 ppm. The remaining peak at 19.2 ppm is assigned to $–CH_3$ from the GT side chain. The MeOH resonance is no longer present in the desolvated state and confirms successful removal of solvent. New resonances at 48.2 and 22.4 ppm can be attributed to $–CH_2-$ and $–CH_3$ environments in different orientation/bonding modes to those in present in the solvated state. Figures 2b,c display the ^{13}C CP/MAS and corresponding PXRD patterns monitoring the progressive changes coupled to desolvation. Upon solvent removal, the MeOH resonance gradually decreases, whilst resonances attributed to the desolvated configuration increase. These intermediate configurations are a mixture of locally ordered solvated and desolvated states. This is in good agreement with the evolution of the PXRD patterns upon guest removal, with the guest-free state retaining similar scattering power and thus crystallinity to the as-grown material consistent with the order seen locally, demonstrating the homogeneous bulk nature of the desolvation process.

The enhanced local order and crystallinity of guest-free ZnGS(75)GT(25) allows the desolvation process to be followed with synchrotron single-crystal X-ray variable-temperature (SCXR-VT), in contrast to the loss of single crystal diffraction from $ZnGA_2$ upon guest loss. After collecting diffraction data for the as-made solvated material at 100K, the crystal was heated to 480K to remove all solvent molecules and cooled to 100K for data collection of the desolvated material. Removal of the guest molecules triggers a cooperative single-crystal-to-single-crystal (SCTSC) rearrangement of the framework from an “open” (O) solvated into a “closed” (C) desolvated state (Fig.3). The hydrogen bonds to the serine sidechain OH are lost upon methanol removal, leaving unoccupied channels across which this uncompensated H-bonding capacity is held apart by the walls, which consist of flexible peptide linkers. The resulting porosity is closed and the lost hydrogen bonding restored simultaneously by torsional changes of the Gly-Ser linker which enable large translational ordered displacements of the peptides. These processes occur cooperatively to retain order both within and between the layers. Whilst C retains the overall metal-to-peptide connectivity of O and displays analogous ..AA.. packing of the layers with equivalent interlayer H-bonds that mediate an interlayer separation of 4.837(5)Å (*cf.* 4.7401(3)Å for O), the edge and diagonal distances separating the metal centers across the opposite sides of the channels within the layers themselves decreases by 0.9, 2.7 (d_1) & 0.1Å (d_2), respectively, and the unit cell volume is reduced by ~180Å^3 (18.6%). This transformation is enabled by the torsional flexibility of GS, which folds to occupy the empty space left by the solvent molecules. The conformation of the peptide changes from Φ = -137.612(2) & Ψ = 167.4872(8)º in O to -132.5(12)º and -77.4(14)º in C, indicating that the folding of the framework is controlled by the rotation of the N-term Gly aa (Ψ) whilst leaving Φ almost unchanged. This is coupled to a translational displacement that compresses the distance between the centroids of the peptides on opposing channel walls by 22.0% (c_1) whilst leaving c_2 almost unchanged (-0.96%). This compression, which reduces the void space in C to 2.9% well below the solvent accessible volume of

27.7% in O, reaches 42.3% when defined as the closest distance separating C3 atoms from opposite amide groups in the unit cell and 60% if considering O11···H9 distances between the atoms involved in host-guest/host-host H-bond formation. The torsion enables the displacement of the two opposite faces of the channel towards each other by allowing the two OH groups to move past each other, which would not be possible with a simple displacement. This increases the density of the structure, and restores the hydrogen bonding lost by removal of the initial methanol guests. This specific conformational change upon guest loss is intrinsic to the introduction of Ser into the dipeptide sequence, as it is driven by the energetically favorable formation of intralayer H-bonds between the side chain hydroxyl and the terminal carboxylate groups of C-terminal residues from peptides on opposite faces of the channel wall in C (O11···H9, 1.9622(18)Å), that energetically counterbalances the breaking of H-bonds between the framework and the guest in O. The combination of torsion and displacement is an ordered variant of the disordered closure mechanism proposed for $ZnGA_2$, driven by the specific directional hydrogen bonding afforded by the serine sidechain and the need to engage these groups in hydrogen bonding. This affords a mechanically stable long-range ordered closed state giving single crystal diffraction, which enables the structure of the closed state to be determined unambiguously. Refinement of the PXRD pattern of desolvated $ZnGS_2$ confirms that it is isostructural to the "closed" state of ZnGS(75)GT(25) and so the structure of the single-peptide phase follows an equivalent structural evolution from porous/open to non-porous/closed as result of dynamical ordered closure upon desolvation.

To understand the evolution in the conformational state of GS that directs its cooperative folding between the ordered, structurally well-defined O and C states, we simulated this process by modelling the removal of methanol molecules from an equilibrated solvated structure with Molecular Dynamics (MD; Fig.4 & SI30). Closing of the structure proceeds via a metastable intermediate configuration (I) located between O and C. First, in less than 1ps, all dipeptides cooperatively adopt conformation I characterized by Φ = - 129.4 & Ψ = -158.0º as –OH groups in Ser take the space previously occupied by methanol molecules. This enables formation of intralayer H-bonds between –OH groups in Ser and the C-term carboxylate group from neighbouring peptides (O···H, 1.88Å), reminiscent of those in C, and is facilitated by changes in orientation of the amine group and valence angles around Zn^{2+}. This folding is also coupled to a displacement of the peptides that squeezes the void space to 6.5% and reduces the distance separating opposite peptides to 5.28Å (*cf.* 9.223(6) and 5.21(3)Å for O & C). In a second stage, the metastable state I gradually evolves to C with all dipeptides adopting their closed conformation over a time of 300ps without the cooperative simultaneous adoption of this state that characterises the transition from O to I. The presence of the OH groups in GS enables ordered closure of the structure, producing a narrower conformational distribution (Fig.SI30d) than that adapted by GA in the disordered $ZnGA_2$ (Fig.SI31d) where the $–CH_3$ group cannot provide equivalent strong and directional hydrogen bonding interactions.

To verify the details of the collapse pathway we conducted DFT calculations of single unit cells with all possible combinations of GS linker conformations seen in states I and C. This confirmed the existence of the metastable state I seen in MD and that higher fractions of C-like conformations lead to more compact and more energetically favourable structures as shown in Fig.4d. The DFT optimization of a unit cell of O after removal of the methanol molecules reveals that the resultant empty structure is energetically unfavourable due to breaking of the H-bonds with the guests. This demonstrates that folding of $ZnGS_2$ is driven by the formation of intraframework H-bonds followed by the relaxation of thermally accessible metastable configurations into the global energy minimum state, C.

Side-chain-enabled ordered closure of the framework. The effect of the OH sidechains extends to the multipeptide MOFs (Fig.5). The dipeptide combinations affording $ZnGT_2$-type topologies remain structurally unchanged after solvent removal and display classical Type I

CO_2 adsorption at 195K (Type R_p; rigid porous). As illustrated in Fig.5b, this behavior is equivalent to that reported for the single-peptide $ZnGT_2$ phase and is determined by the robustness of the frameworks, which remain intact upon evacuation. Micropore volumes, calculated for the maximum uptake at 1bar, vary from 0.112 to 0.109 $cm^3.g^{-1}$ (SI66) and are consistent with the value of 0.093$cm^3.g^{-1}$ calculated from the crystal structure of desolvated $ZnGT_2$.[17] Isosteric heats of adsorption (Q_{st}) were calculated by fitting the adsorption branches at 273 and 298K to a virial-type expression.[22] Values at zero coverage suggest that the frameworks display a higher affinity for CO_2 at increasing levels of GT doping.

All of the solids adopting the GS/GA structure undergo dynamical ordered closure upon guest loss. Even 10% GS substitution into $ZnGA_2$ is sufficient to drive ordered closure by nucleating the cooperative torsional change required through hydrogen bonding. Within this flexible (F) class, there are two categories of behavior. Structures adopting this topology where all the dipeptides have hydrogen bonding sidechains (GS, GS:GT for GS ≥ 50%) remain closed to CO_2 at pressures up to 15 bar (the highest measured), in contrast to $ZnGA_2$ which admits CO_2 above a gate pressure of 0.2 bar at 195K and 2 bar at 273K. The interaction of CO_2 molecules with $ZnGS_2$ (and the isostructural all-OH sidechain materials) is not strong enough to break the sidechain to carboxylate H-bonds stabilizing the closed state and trigger the re-opening of the pores up to 15 bar at 273K. However, exposure to the polar guest MeOH results in uptake to re-form the open structure driven by the formation of sidechain–guest H-bonds (Fig.5e). These materials are classified as flexible non-porous F_{npCO2} in recognition of their closure to CO_2 over the studied conditions.

In contrast, $Zn(GS/GA)_2$-structured materials containing GA will adsorb CO_2 above a temperature-dependent gate pressure P_{go} which is controlled by the amount of GA present. This is consistent with the methyl sidechain of GA disrupting the H bonding network sufficiently to permit opening of the structure in the presence of CO_2, which has weaker guest-host interactions than the H-bonding methanol which is required to open the all-H-bonded sidechain GS/GT materials with this structure. Comparison of the experimental CO_2 isotherms of $ZnGA_2$, ZnGA(75)GS(25) and ZnGA(75)GT(25) at 195K (Fig.5c) reveals an increased gate pressure from 35mbar ($ZnGA_2$) to 125 and 240mbar. This gate pressure is higher for an equivalent amount of GT than GS, demonstrating that H-bonding involving Thr is more effective in closing the structure than that involving Ser. By comparing the chemical potential of CO_2 at P_{go} for the GA:GS dyad, we found that, compared to $ZnGA_2$, the additional free energy required to open the closed structure increases linearly with the content of GS (SI33). This gives rise to an exponential dependence of P_{go} with the concentration of GS shown in Fig.5d. The model predicts that $ZnGS_2$ will remain closed up to an inaccessible P_{go} of 17 bar at 195K, consistent with the observed behavior. These materials are denoted as F_{pCO2} (flexible porous to CO_2).

The distinct structural responses to CO_2 of the all H-bonding sidechain F_{npCO2} materials and the $–CH_3$ sidechain-containing F_{pCO2} compounds was demonstrated by in-situ gas-cell synchrotron PXRD measurements on increasing the CO_2 pressure to 10 bar and then decreasing it (Fig.5f) on two compositions that are isostructural when desolvated as both adopt the C structure of $ZnGS_2$: the F_{npCO2} ZnGS(75)GT(25) and the F_{pCO2} ZnGA(75)GT(25). The PXRD pattern of the ZnGS(75)GT(25) remains unchanged for the whole interval of pressures studied confirming that the structure remains closed up to 10 bar, in good agreement with the sorption measurements. In contrast, ZnGA(75)GT(25) displays a progressive re-opening of the structure upon gas loading, reaching approximately 50% conversion at 10 bar and approximately 90% at 15 bar (Fig.SI68). Reduction of the pressure from 15 bar leads to reversible closure of the structure. These data show that the ordered torsional changes closing the porosity can be reversed by CO_2 above a gate pressure to open the structure when methyl sidechains disrupt the hydrogen bonding pattern responsible for stabilising the closed structure, but not when there is a complete set of sidechain to C-terminal carboxylate

hydrogen bonds favouring the closure structure of every potential guest location. The interactions between the sidechains within the solid solution structures produce synergic effects that give guest response which is not a linear combination of the two end-members *e.g.* both $ZnGA_2$ and $ZnGT_2$ are open to CO_2 at 195K at pressures below 0.2 bar ($ZnGT_2$ is open at all pressures) but ZnGA(50)GT(50) is closed up to the maximum measured pressure of 15 bar because the GA concentration drives the material into the GA/GS structure type, and the GT imposes ordered closure upon guest loss into the GS C structure which is locked closed by the Thr-based sidechain to carboxylate hydrogen bonding. The GA thus changes the GT-based structure to a GA-based one, and the GT imposes non-GA properties to give a non-linear change in performance with respect to the end-member compounds.

The torsional degrees of freedom of the GS dipeptide reposition the OH-bearing sidechain of the Ser residue to enable a large translational displacement of the peptide. These coupled motions form a hydrogen bond that closes the structure of $ZnGS_2$ on guest loss in an ordered manner driven by this conformational change, affording a mechanically stable and translationally symmetric closed state where the lost hydrogen bonding to the guest is compensated by the new host-host interaction. This contrasts with the disordered closure of $ZnGA_2$ where the absence of directional bonding associated with the methyl sidechain of Ala offers no unique closure path. The strength of the resulting hydrogen bond makes the structure openable only by polar guests rather than the CO_2-accessible porosity offered by the isostructural $ZnGA_2$ and the rigid $ZnGT_2$, demonstrating the changes in function associated with a difference in one amino acid residue that result from coupling of sidechain functionality to torsional changes. Crystallinity is retained despite these large displacements due to the ordered nature of the closure favoured by the directional nature of the hydrogen bonds that drive it. In proteins, coupled torsional and translational displacements are associated with folding into conformations appropriate for a given environment and function, and single point mutations can radically alter structure and function. For example, the Drosophila GABA receptor displays insecticide resistance when Ala is exchanged with Ser whilst this is reduced by Thr to Ala mutation.[23,24] The sidechain control of $ZnXY_2$ dipeptide framework function permits the tuning of their properties over a wide range through the formation of multipeptide solid solutions which display non-linear property variations due to synergic interactions between the functional groups on the constituent peptides, setting the challenge of ordering the assembly of these multiple peptides within solids to access new properties.

References

1 See special issue on Metal-Organic Frameworks *Chem. Rev.* **112**, 673-1268 (2012).

2 Li, J. R., Kuppler, R. J. & Zhou, H. C. Selective gas adsorption and separation in metal–organic frameworks. *Chem. Soc. Rev.* **38**, 1477–1504 (2009).

3 Yang, W. *et al.* Selective CO_2 uptake and inverse CO_2/C_2H_2 selectivity in a dynamic bifunctional metal–organic framework. *Chem. Sci.* **3**, 2993 (2012).

4 Dhakshinamoorthy, A. & García, H. Catalysis by metal nanoparticles embedded on metal–organic frameworks. *Chem. Soc. Rev.* **41**, 5262 (2012).

5 Lee, J.-Y. *et al.* Metal–organic framework materials as catalysts. *Chem. Soc. Rev.* **38**, 1450–1459 (2009).

6 Rocca, Della, J., Liu, D. & Lin, W. Nanoscale Metal-Organic Frameworks for Biomedical Imaging and Drug Delivery. *Acc. Chem. Res.* **44**, 957–968 (2011).

7 Bauer, C. A. *et al.* Influence of connectivity and porosity on ligand-based luminescence in zinc metal-organic frameworks. *J. Am. Chem. Soc.* **129**, 7136–7144 (2007).

8 Ferrando-Soria, J. *et al.* Highly Selective Chemical Sensing in a Luminescent Nanoporous Magnet. *Adv. Mater.* **24**, 5625–5629 (2012).
9 Deng, H. *et al.* Large-Pore Apertures in a Series of Metal-Organic Frameworks. *Science* **336**, 1018–1023 (2012).
10 Guillerm, V. *et al.* A Series of Isoreticular, Highly Stable, Porous Zirconium Oxide Based Metal-Organic Frameworks. *Angew. Chem. Int. Ed.* **51**, 9267–9271 (2012).
11 Hasegawa, S. *et al.* Three-dimensional porous coordination polymer functionalized with amide groups based on tridentate ligand: Selective sorption and catalysis. *J. Am. Chem. Soc.* **129**, 2607–2614 (2007).
12 Barrio, J. *et al.* Control of porosity geometry in amino acid derived nanoporous materials. *Chem-Eur J.* **14**, 4521–4532 (2008).
13 An, J., Geib, S. J. & Rosi, N. L. High and Selective CO_2 Uptake in a Cobalt Adeninate Metal− Organic Framework Exhibiting Pyrimidine-and Amino-Decorated Pores. *J. Am. Chem. Soc.* **132**, 38–39 (2009).
14 Imaz, I. *et al.* Metal–biomolecule frameworks (MBioFs). *Chem. Commun.* **47**, 7287 (2011).
15 Boehr, D. D., Nussinov, R. & Wright, P. E. The role of dynamic conformational ensembles in biomolecular recognition. *Nat. Chem. Biol.* **5**, 789–796 (2009).
16 Rabone, J. *et al.* An adaptable peptide-based porous material. *Science* **329**, 1053–1057 (2010).
17 Martí-Gastaldo, C., Warren, J. E., Stylianou, K., Flack, N. L. O. & Rosseinsky, M. J. Enhanced Stability in Rigid Peptide-Based Porous Materials. *Angew. Chem. Int. Edit* **51**, 11044–11048 (2012).
18 Deng, H. et al. Multiple Functional Groups of Varying Ratios in Metal-Organic Frameworks. *Science* **327**, 846-850 (2010).
19 Fukushima, T. *et al.* Solid Solutions of Soft Porous Coordination Polymers: Fine-Tuning of Gas Adsorption Properties. *Angew. Chem. Int. Edit* **49**, 4820–4824 (2010).
20 Burrows, A. D. Mixed-component metal–organic frameworks (MC-MOFs): enhancing functionality through solid solution formation and surface modifications. *CrystEngComm* **13**, 3623 (2011).
21 Henke, S., Schneemann, A., Wütscher, A. & Fischer, R. A. Directing the Breathing Behavior of Pillared-Layered Metal–Organic Frameworks via a Systematic Library of Functionalized Linkers Bearing Flexible Substituents. *J. Am. Chem. Soc.* **134**, 9464–9474 (2012).
22 Czepirski, L. & Jagiello, J. Virial-Type Thermal Equation of Gas Solid Adsorption. *Chem. Eng. Sci.* **44**, 797–801 (1989).
23 Ffrench-Constant, R. H., Rocheleau, T. A., Steichen, J. C. & Chalmers, A. E. A point mutation in a Drosophila GABA receptor confers insecticide resistance. *Nature* **363**, 449-451(1993).
24 Altschmied, L., Baumeister, R., Pfleiderer, K. & Hillen, W. A threonine to alanine exchange at position 40 of Tet repressor alters the recognition of the sixth base pair of tet operator from GC to AT. *EMBO J.* **7,** 4011-4017 (1988).

Acknowledgements

Research was supported by EPSRC under EP/H000925. CMG thanks the EU for a Marie Curie Fellowship (IEF-253369). Via our membership of the UK's HPC Materials Chemistry Consortium, funded by EPSRC (EP/F067496), this work made use of the facilities of HECToR, the UK's national high-performance computing service.

Additional information

Supplementary information is available in the online version of the paper. Reprints and permission information is available online at http://www.nature.com/reprints. Correspondence and requests for materials should be addressed to M.J.R.

Figure 1. Structure of as-made $ZnGS_2$ (a) Chemical structure of the peptide, tetrahedral coordination of the Zn (II) ion and peptide-to-metal connectivity in the solvated structure of [Zn(Gly-Ser)$_2$]. (b) Square-like structure viewed along the *c* axis. The resulting pockets are filled with methanol molecules in the solvated material. See SI25 for a theoretical description of the location of MeOH molecules in the structures of solvated GS_2 and GA_2.(c) ß-sheet packing of the layers as imposed by the H-bonds (represented by red dashed lines) involving. N-H and C=O groups from neighboring layers (d) One-dimensional channels running parallel to [001]. (e) Bilobal "hourglass" shaped pore imposed by the projection of the hydroxyl groups from the $–CH_2OH$ side chain of the L-serine units. Zn, dark blue; O, red; C, grey; N, blue; H, white.

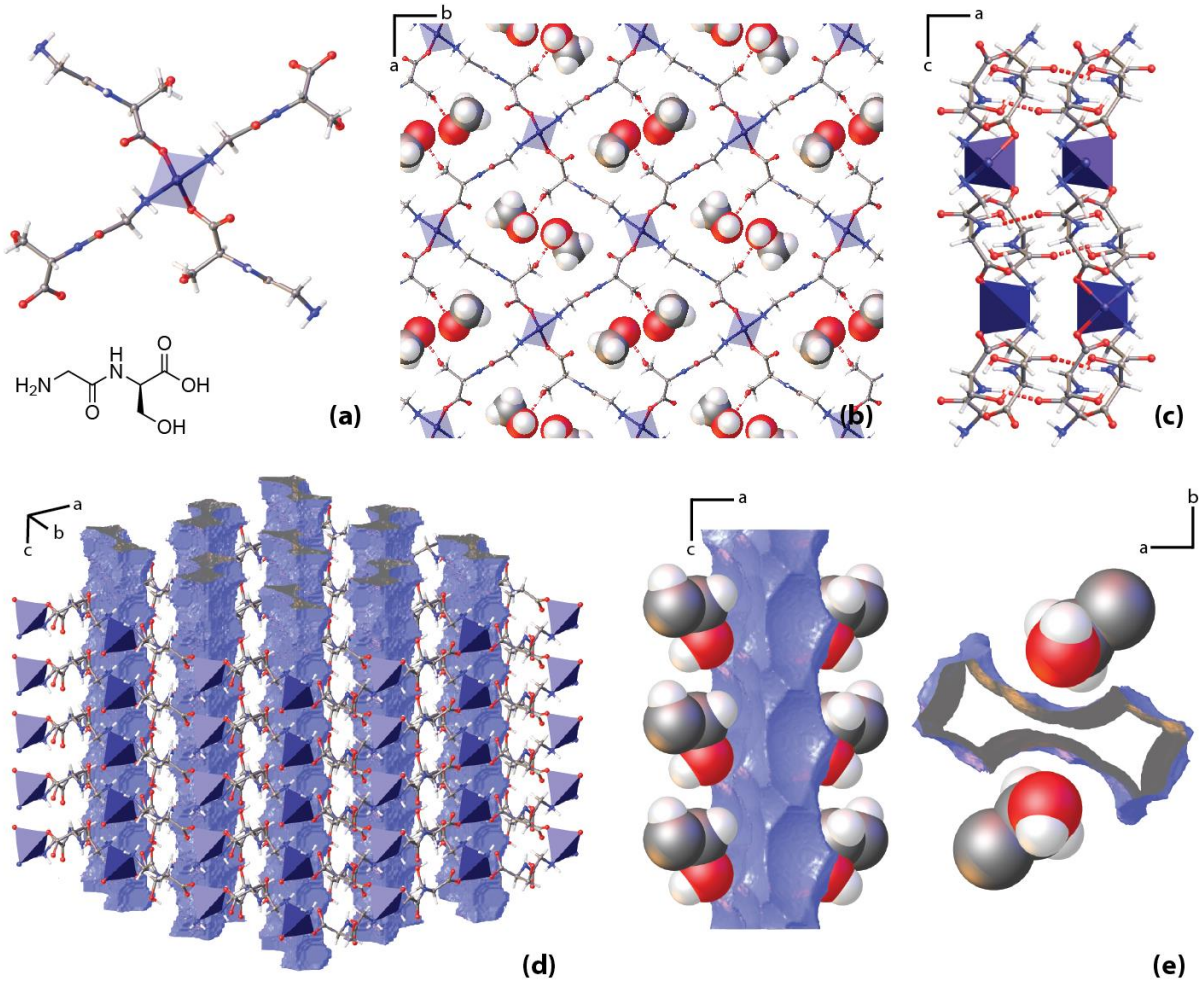

Figure 2. Ordered nature of the local environment in solvated and desolvated ZnGS(75)GT(25) (a) Solid-state ^{13}C CP/MAS NMR of as-made (top) and desolvated (bottom) ZnGS(75)GS(25) at room temperature that confirm the preservation of local order upon solvent removal. The table summarizes the assignment of the spectra (see text for more details). Evolution of the ^{13}C CP/MAS NMR spectra (b) and PXRD (c) of ZnGS(75)GS(25) upon progressive solvent removal: as-made (100% open), overnight evacuation at room temperature (83.9(4)% open), evacuation at 60ºC for 48hrs (14.8(7)% open) and evacuation at 60ºC for 48hrs under N_2 followed by packing in the glove box (0% open). Observed (black), calculated (red) and difference (grey) profiles from Rietveld refinement used to calculate the relative phase percentages are shown (see SI4 for more details). Tick marks indicate the Bragg reflections for the "open" (blue) and "closed" (black) structures. Most intense diffraction lines characteristic of the "open" and "closed" states are highlighted in grey.

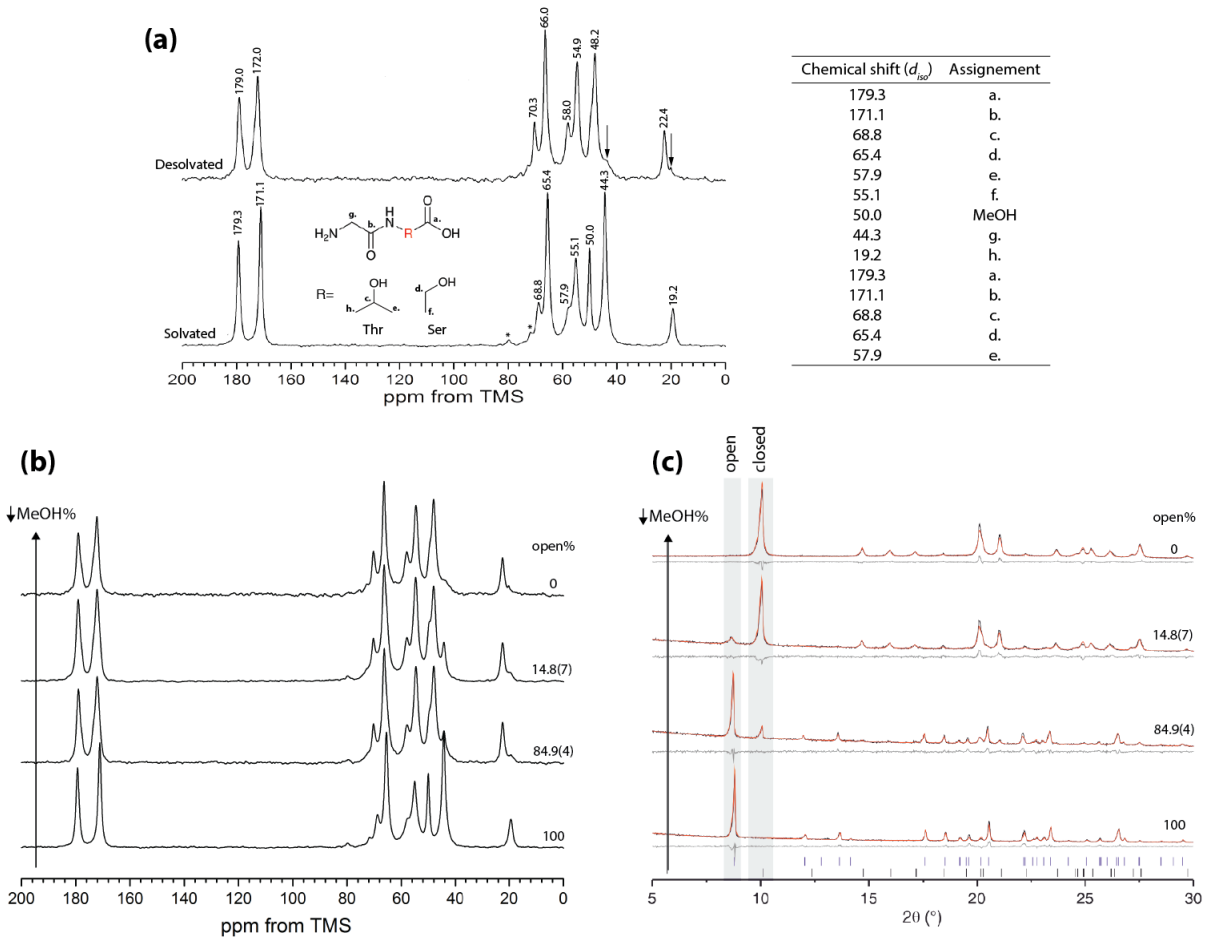

Chemical shift (d_{iso})	Assignement
179.3	a.
171.1	b.
68.8	c.
65.4	d.
57.9	e.
55.1	f.
50.0	MeOH
44.3	g.
19.2	h.
179.3	a.
171.1	b.
68.8	c.
65.4	d.
57.9	e.

Figure 3. Structure of desolvated ZnGS(75)GT(25) and metrics of the SCTSC transformation (a) Tetrahedral coordination of the Zn (II) ion and peptide-to-metal connectivity upon solvent removal in ZnGS(75)GT(25). New intralayer H-bonds formed upon the framework closure are highlighted as dashed red lines. (b) Rectangle-like structure of the neutral layers along the c axis. (c) ß-sheet packing of the layers as imposed by the H-bonds involving N-H and C=O groups from neighboring layers which are preserved upon guest loss (dashed bonds in blue). (d) Metrics of the SCTSC open-to-close transformation highlighting the changes in the intercation distances -edge (orange) & diagonals d_1 & d_2 (purple)- and peptide-to-peptide separation defined as: distance between peptides' centroids from opposing walls (c_1 & c_2; green), closest distance separating C3 atoms from opposite amide groups (blue) and O11⋯H9 distances between the atoms involved in host-guest/host-host H-bond formation (red). Zn, dark blue; O, red; C, grey; N, blue; H, white. For clarity we have not distinguished between the positions of the sidechain –H and $–CH_3$ substituents associated with the GS and GT residues.

(a)

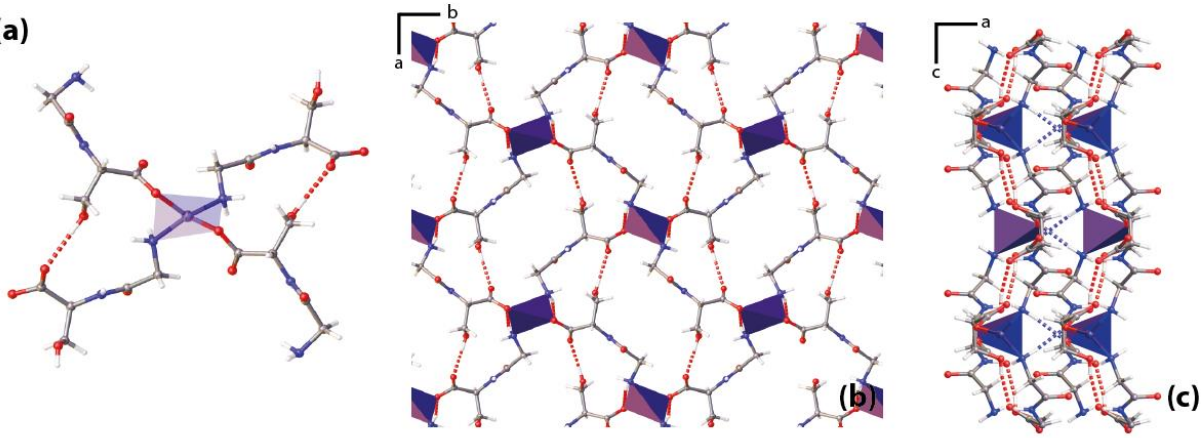

(d)

	Zn-Zn distance /Å			peptide-peptide distance /Å			
	edge	(d_1)	(d_2)	(c_1)	(c_2)	C3---C3	O11---H9
Open (O)	10.1442(5)	13.8808(10)	14.6838(11)	8.205(2)	12.101(3)	9.223(6)	4.919(3)
Closed (C)	9.214(7)	11.151(12)	14.586(16)	6.398(10)	12.217(12)	5.21(3)	1.962(10)

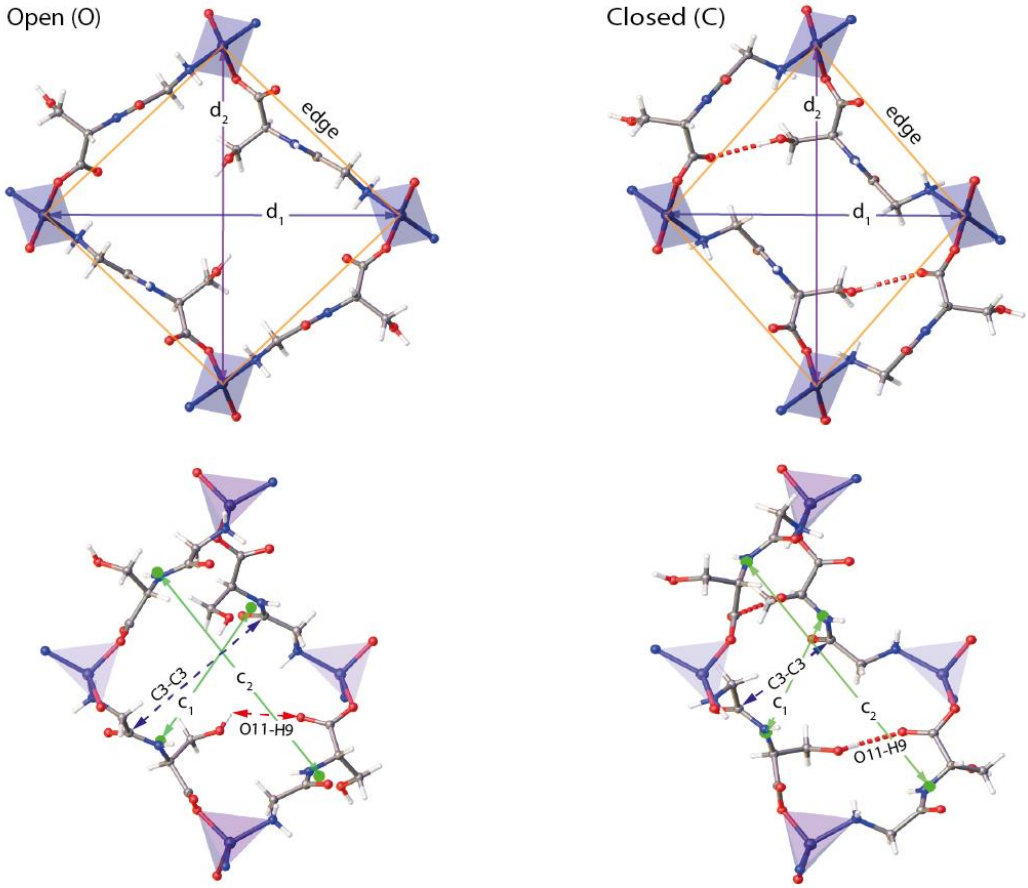

Figure 4. Computational modeling of the cooperative peptide folding closure mechanism (a) Comparison of the structure of ZnGS(75)GT(25) in the open (O), intermediate (I) and closed (C) states displaying the folding of the peptide coupled to reduction of the porosity shown by representation of the Connolly surfaces. O and C correspond to SCXR-VT experiments whilst I was identified in MD simulations of the guest-loss and closure process. The change in the peptide translational state has been defined as the closest distance separating C3 atoms from opposite amide groups in the unit cell. (b) Overlaid representation of the different conformations adopted by the GS dipeptide upon ordered closure. (c) Overlaid free energy profiles in the (Φ,Ψ) plane calculated from MD simulations of the C and O phases in equilibrium. There is a single energy minimum in phase O, whereas both conformations I (metastable) and C (stable) can be observed for phase C. The contour lines correspond to 1, 2 and 3 k_BT at 298K. (d) Relative energies and the distance separating opposite peptides in a unit cell containing 4 GS peptides in different conformations calculated with DFT. C, I and O denote unit cells with all 4 peptides in respectively closed, intermediate and open conformation, while numbers correspond to the number of intermediate peptides present for mixed I/C states. See SI26 for more details.

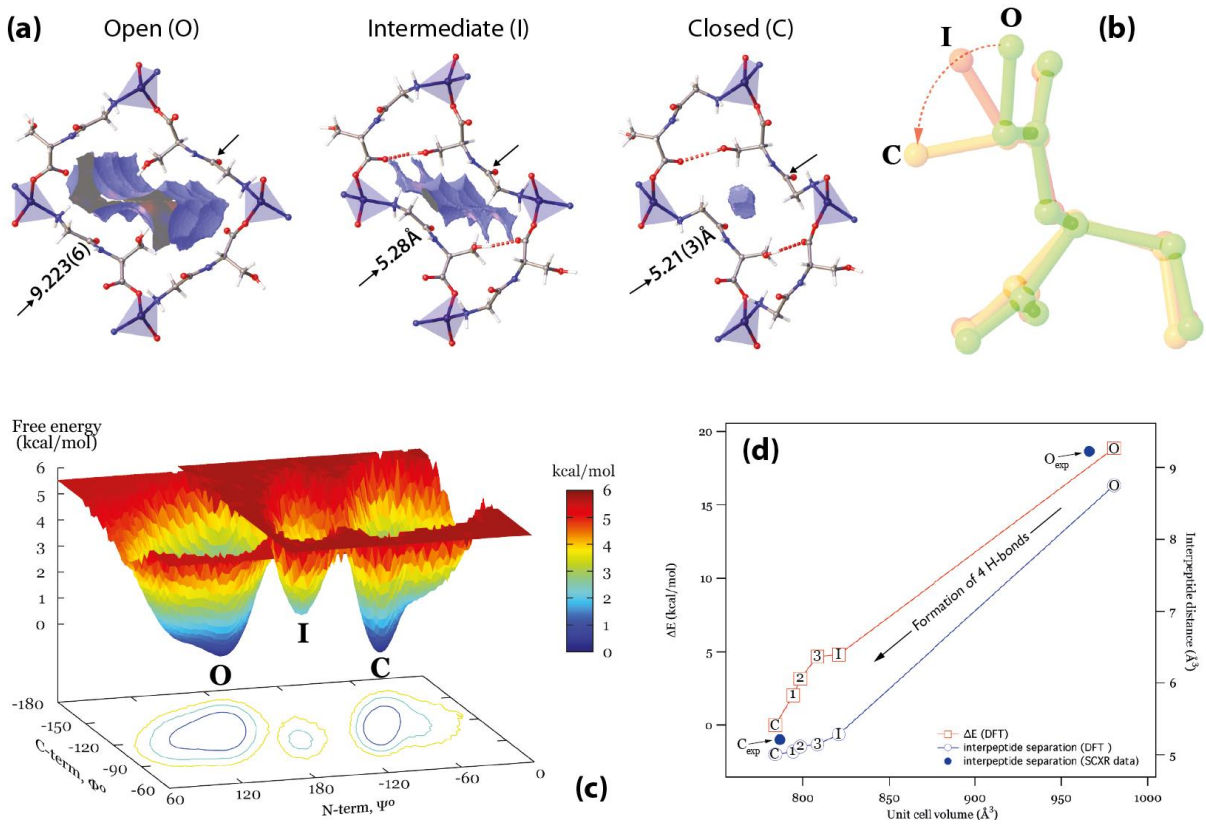

Figure 5. Porosity and powder diffraction data of $ZnGS_2$ and multiple peptide MOFs (a) Ternary diagram summarizing the overall structure and highlighting the three different types of CO_2 porosity in the multipeptide MOFs as controlled by the relative dipeptide-to-dipeptide ratios: rigid porous (R_p, black), flexible non-porous to CO_2 (F_{npCO2}, grey) and flexible porous to CO_2 (F_{pCO2}, color gradient is connected to variation in the gate opening pressure). Filled dots and squares stand for $Zn(GS/GA)_2$ and $ZnGT_2$ topologies, respectively. (b) CO_2 isotherms at 195K of the R_p: ZnGA(25)GT(75) (circles), ZnGS(50)GT(50) (triangles) and ZnGS(25)GT(75) (squares). Inset: Isosteric heats of adsorption calculated from the adsorption branches at 273 and 298K with a virial-type expression. (c) CO_2 isotherms at 195K of $ZnGA_2$ (circles) and the F_{pCO2}: ZnGA(90)GS(10) (triangles), ZnGA(75)GS(25) (squares), ZnGA(75)GT(25) (tilted triangles), ZnGA(60)GS(40) (diamonds) and Zn-GA(50)GS(50) (inverted triangles). Filled and empty symbols stand for adsorption and desorption, respectively. (d) Variation of P_{go} with GA doping for the GA:GS dyad. Inset displays the linear regime followed by the additional free energy required to open the closed structure with GS%. Red solid lines stand for the best fit of the experimental data to the theoretical model described in SI33. (e) PXRD patterns of $ZnGS_2$: as-made (red), after overnight evacuation (black) and after controlled exposure to MeOH vapors (blue). (f) In-situ Synchrotron PXRD of a) F_{pCO2} ZnGA(75)GT(25) and b) F_{npCO2} ZnGS(75)GT(25). Samples were measured as-made (red), desolvated (black) and under a pressure of approximately 10 bar CO_2 (green). Powder diffraction data is shown as a function of scattering vector, $Q = 4\sin\theta/\lambda$. See SI4 for details and SI34-48 for refinement of the PXRD data and calculated unit cell parameters. Most intense diffraction lines characteristic of the "open" and "closed" states are highlighted in gray.

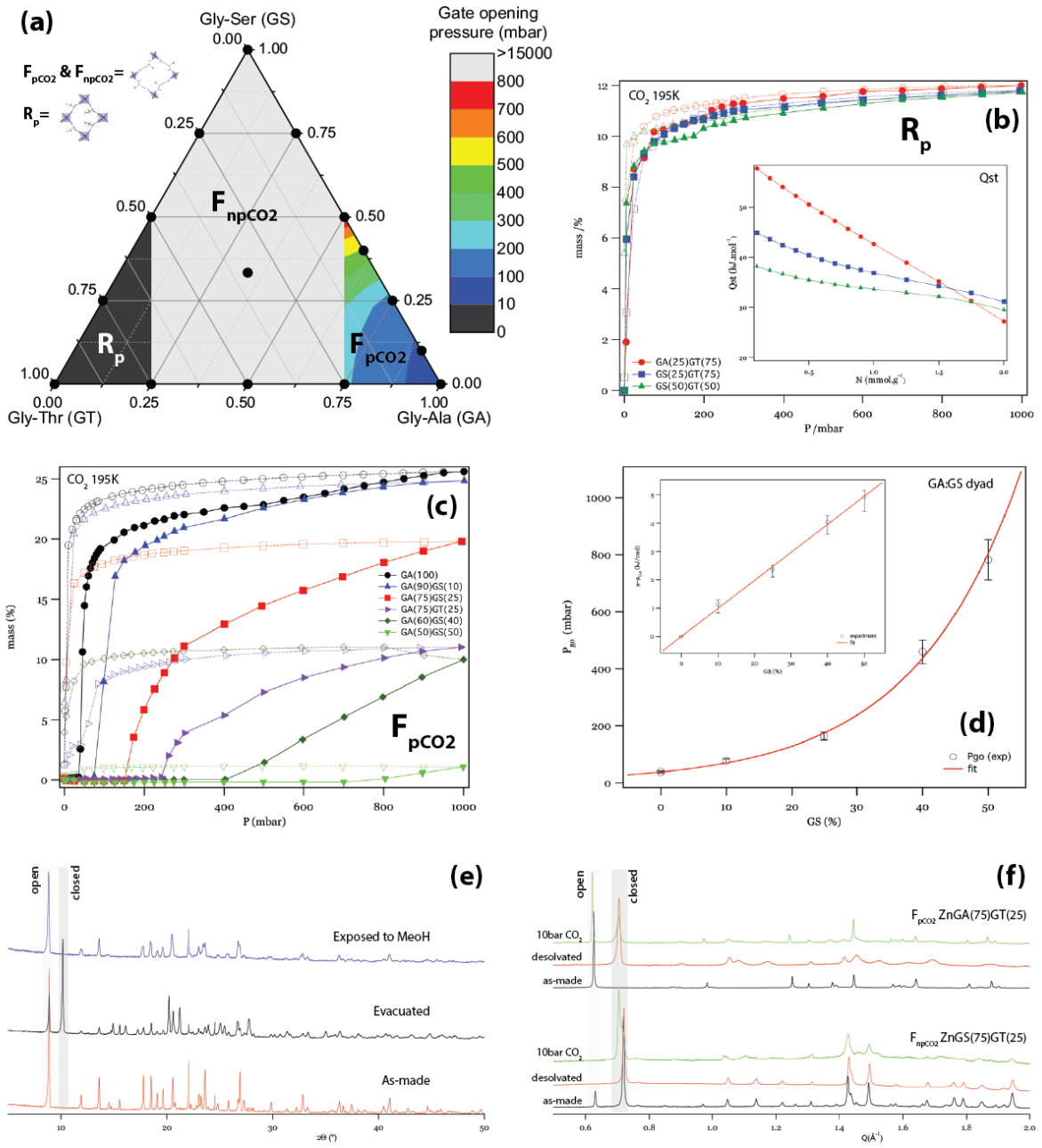
(a)
Gly-Ser (GS)
Gate opening pressure (mbar)
>15000
800
700
600
500
400
300
200
100
10
0
F_pCO2 & F_npCO2 =
R_p =
F_npCO2
R_p
F_pCO2
Gly-Thr (GT)
Gly-Ala (GA)
(b)
CO2 195K
R_p
Qst
mass /%
P /mbar
GA(25)GT(75)
GS(25)GT(75)
GS(50)GT(50)
(c)
CO2 195K
mass (%)
P (mbar)
GA(100)
GA(90)GS(10)
GA(75)GS(25)
GA(75)GT(25)
GA(60)GS(40)
GA(50)GS(50)
F_pCO2
(d)
GA:GS dyad
P_go (mbar)
GS (%)
Pgo (exp)
fit
(e)
open
closed
Exposed to MeoH
Evacuated
As-made
2θ (°)
(f)
open
closed
F_pCO2 ZnGA(75)GT(25)
10bar CO2
desolvated
as-made
F_npCO2 ZnGS(75)GT(25)
10bar CO2
desolvated
as-made
Q(Å-1)